J Biomol NMR (2008) 42:279–286
DOI 10.1007/s10858-008-9282-y

NMR STRUCTURE NOTE

Refinement of the solution structure and dynamic properties of Ca^{2+}-bound rat S100B

Nathan T. Wright · Keith G. Inman · Jonathan A. Levine · Brian R. Cannon · Kristen M. Varney · David J. Weber

Received: 21 August 2008 / Accepted: 3 October 2008 / Published online: 24 October 2008

Biological context

The small (~10.5 kDa) acidic Ca^{2+}-binding protein S100B belongs to the S100 protein family, a group of over 20 members that share significant sequence homology and undergo a large conformational change upon the addition of calcium. S100 proteins have no intrinsic enzymatic activity; instead, a Ca^{2+}-dependent conformational change enables them to bind and modulate the activity of a diverse pool of intracellular target proteins. For S100B, these include cytoskeletal and filament associated proteins (e.g. tubulin, GFAP, tau, desmin, vimentin, CapZ, calponin, calpactin I, and caldesmon), other Ca^{2+}-binding proteins (annexins II, V, VI, S100A1, S100A6, S100A11, and neurocalcin-δ), membrane associated proteins (neuromodulin, neurogranin, MARCKS, giant protein AHNAK, and IQGAP1), transcription factors and their regulators (e.g. p53, hdm4, and hdm2), and several enzymes (e.g. aldolase, phosphoglucomutase, photoreceptor guanyl cyclases, Ndr kinase, and protein kinase C) (reviewed in Wilder et al. 2006). In addition, S100B is secreted from the cell under stress conditions and targets cell surface receptors such as RAGE in the extracellular environment (reviewed in Heizmann et al. 2007).

Several S100 proteins, including S100B, are up-regulated in response to various pathologies including Alzheimer's disease, Down's syndrome, and a number of malignancies, and are used as disease markers and prognostic indicators. Mechanistic studies suggest that S100B and perhaps other S100 proteins contribute to these diseases. For example in cancers such as malignant melanoma, anaplastic astrocytomas, and glioblastomas, high concentrations of S100B correlate directly with very low protein levels of wild-type p53 tumor suppressor (reviewed in Salama et al. 2008). Upon further examination, it was found that S100B binds p53 in a Ca^{2+}-dependent manner, significantly reducing p53 protein levels and inhibiting wild-type p53 functions (Lin et al. 2004; Rustandi et al. 2000). Likewise, siRNA inhibition of S100B production restores wild-type p53 protein levels and its activities (i.e. cell cycle regulation, apoptosis) as necessary to restore normal tumor suppression functions (Lin et al. 2004). Thus, as with other negative regulators of p53 (i.e. hdm2), efforts are currently underway to design small molecule inhibitors that specifically bind to the Ca^{2+}-bound form of S100B and block the S100B-p53 interaction as a potential therapeutic strategy to treat cancers with wild-type p53 and elevated S100B (Charpentier et al. 2008). For such drug design efforts to be successful, it is important to fully understand the structural and dynamic properties of Ca^{2+}-bound S100B.

While several NMR and X-ray crystal structures of Ca^{2+}-S100B are available (Drohat et al. 1998; Matsumura et al. 1998; Smith and Shaw 1998; Wilder et al. 2006), there is a discrepancy with regard to the conformation of the last eight residues in its C-terminus. In the X-ray crystal

Electronic supplementary material The online version of this article (doi:10.1007/s10858-008-9282-y) contains supplementary material, which is available to authorized users.

N. T. Wright · K. G. Inman · J. A. Levine · B. R. Cannon · K. M. Varney · D. J. Weber (✉)
Department of Biochemistry and Molecular Biology, University of Maryland School of Medicine, 108 N. Greene St, 21201 Baltimore, MD, USA
e-mail: dweber@umaryland.edu

K. G. Inman
Department of Pediatrics, Center for Vaccine Development, 685 W. Baltimore St, 21201 Baltimore, MD, USA

structure, helix 4 is extended to include nearly the entire end of the molecule (to F88), which is different from the published NMR structures in which helix 4 ends at A83 with the remaining eight residues considered part of the C-terminal loop (loop 4). The importance of this region for binding p53 and other protein targets is well-established (Inman et al. 2002), so the structural and dynamic properties of this portion of Ca^{2+}-S100B need to be clearly understood. To this end, we have refined the solution NMR structure of rat Ca^{2+}-S100B by including long-range residual dipolar coupling (RDC) constraints. In addition, ^{15}N-relaxation data for backbone amide groups are presented here. Together, these new data provide direct evidence that residues at the C-terminus of Ca^{2+}-S100B (C84-E91), as well as several residues in loop 2 (termed the hinge region), are not fully structured, but rather are dynamic in solution. That these residues are flexible is likely a necessary characteristic of Ca^{2+}-S100B for accommodating its interaction with a large number of protein targets.

Methods and results

Materials

Deuterated MES, D_2O, $^{15}NH_4Cl$, and ^{13}C-glucose were purchased from Cambridge Isotopes Laboratories (Woburn, MA). Other materials were of the highest commercial quality and passed through Chelex-100 resin (BioRad) to remove trace metals.

Sample preparation

^{15}N-labeled S100B or ^{15}N, ^{13}C-labeled S100B was overexpressed and purified from *Escherichia coli* as previously described (Inman et al. 2001). While apo-S100B is dimeric in solution at millimolar concentrations, there was evidence of higher order aggregates in samples of Ca^{2+}-S100B prepared at subunit concentrations above 1 mM. However, at concentrations below 600 μM, no aggregation was detected and R_2 values for backbone ^{15}N resonances throughout the protein did not change as a function of protein concentration. Specifically, the average trimmed mean R_2 values at 14.4 T were 17.1 ± 1.6 s^{-1} at 1.3 mM, 16.6 ± 1.7 s^{-1} at 900 μM, 15.8 ± 1.9 s^{-1} at 600 μM, and 15.7 ± 1.9 s^{-1} at 400 μM protein concentrations, respectively. Furthermore, individual R_2 values for all residues were indistinguishable within error (<4% different) at 600 and 400 μM S100B subunit concentration. Therefore, NMR experimental collection of both the structural and ^{15}N-relaxation rate data were conducted at 400 μM S100B, 5 mM $CaCl_2$, 25 mM NaCl, 10 mM DTT, 10 mM MES, pH 6.7. All samples were degassed by vacuum and argon replacement shortly before each experiment. For partial alignment, necessary for collecting RDC data, a 2× stock of the Ca^{2+}-S100B protein/buffer solution was soaked into a cylindrical 5% acrylamide gel overnight to give a final S100B concentration of 400 μM. This gel was then radially compressed (i.e. stretched) or axially compressed to obtain the aligned samples, as previously described (Wright et al. 2005, 2008).

NMR data collection

NMR spectra were collected at 37°C with a Bruker DMX600 NMR spectrometer (600.13 MHz for protons) and a Bruker AVANCE 800 NMR spectrometer (800.27 MHz for protons) equipped with four frequency channels and a triple-resonance z-axis gradient 5 mm cryoprobe. As reported previously for apo-S100B (Inman et al. 2001), ^{15}N-relaxtion rate data (T_1, T_2, heteronuclear NOE) were also examined for Ca^{2+}-S100B, so backbone dynamics could also be considered for the state in which this protein binds its targets. Specifically, backbone ^{15}N T_1 and T_2 spectra were acquired with 32 scans per t_1 point at both 600 and 800 MHz. A recycle delay of 3.0 s was used at both fields. T_1 delay times of 30 (x2), 70 (x2), 130, 200, 300, 480, and 960 ms were used for data collection at 600 MHz, and 30 (x2), 70 (x2), 100, 200, 300, 400, and 500, 600, and 900 ms at 800 MHz. T_2 delay times of 16 (x2), 24, 32 (x2), 40, 48, 56, and 64 ms were used for data collection at 600 MHz, and 10 (x2), 20 (x2), 30, 40, 50, 60, and 70 ms at 800 MHz. {^{1}H}-^{15}N NOE ratios were measured with a 3-s pre-saturation period and a 2-s relaxation delay; the control experiment had an equivalent 5-s delay. Both NOE and control experiments were acquired in an interleaved fashion, with 56 scans at 600 MHz and 48 scans at 800 MHz and with 256 t_1 points.

NMR data processing and analysis

All NMR data were processed and analyzed with NMRPipe and NMRDraw software (Delaglio et al. 1995), as previously described (Inman et al. 2001). Data was extended in the indirect dimension (t_1) by linear prediction, using a prediction order of no more than one-third the number of complex points and zero-filled in both dimensions to double the number of points. Apodization with a 5%-shifted mixed Gaussian/exponential function was applied with weighting chosen to reproduce the natural line width values. For the relaxation series, correlations with S/N > 15 were selected and peak heights were measured by fitting Gaussian surfaces to the transformed data and taking the maximum height of the fitted surface using the program NLINLS (Delaglio et al. 1995). The jackknife

procedure was used with the Levenberg-Marquardt non-linear least squares algorithm to fit peak heights, using the computer program CURVEFIT (A.G. Palmer, Columbia University). Peak heights for the heteronuclear NOE and reference experiments were also extracted from Gaussian fits to the frequency-domain data as previously described (Inman et al. 2001).

Structure calculations

Residual dipolar coupling data ($^1D_{NH}$ and $^1D_{C\alpha H\alpha}$) were collected in order to refine the solution NMR structure of Ca^{2+}-bound S100B (Drohat et al. 1998). Specifically, 2D IPAP ^1H-^{15}N HSQC experiments were used to record ^{15}N-H^N splittings, and 3D CT-(H)CA(CO)NH experiments without H_α decoupling during C_α acquisition in t_2 were used to record $^{13}C_\alpha$-H_α splittings. Residual dipolar coupling values (in Hz) were determined by measuring the difference in J splitting between data collected under conditions with isotropic tumbling and analogous data collected with partially aligned samples. The RDCs were incorporated into structure calculations using alignment tensors generated from data collected under two alignment conditions as previously described (Tjandra et al. 1997; Bax et al. 2001; Wright et al. 2005). $^1D_{NH}$ and $^1D_{C\alpha H\alpha}$ data from a radially compressed gel (i.e. stretched gel) were fit simultaneously to enforce a single alignment tensor ($A_a \sim 0.6 \times 10^{-3}$) since these data were collected under the same conditions. A second $^1D_{NH}$ data set was also collected in an axially compressed gel ($A_a \sim 0.6 \times 10^{-4}$), and these data slightly improved the overall quality of the structures. The Q-factor reported for the family of structures was calculated twice and the average value is listed in Table 1 ($Q = 0.19 \pm 0.02$; Table 1). In each calculation, 10% of the $^1D_{NH}$ and 10% of the $^1D_{C\alpha H\alpha}$ RDCs from the radially compressed gel were randomly removed and then used to calculate the Q-factor, as described (Bax et al. 2001; Wright et al. 2005). Most structures (>180 of 200) had no NOE or dihedral violations, and many (>75) displayed a high level of convergence (backbone rmsd <0.85). The final 20 structures were selected based on lowest energy and were of high quality based on the statistical criteria listed in Table 1. The coordinates of the refined solution structure of Ca^{2+}-S100B have been deposited in the Protein Data Base (PDB identification code: 2K7O), and the T_1, T_2, NOE, and RDC values were deposited at the BMRB under the accession code 15923.

Refined solution structure of Ca^{2+}-S100B

The solution NMR structure of dimeric Ca^{2+}-S100B reported previously (Drohat et al. 1998) was refined by the inclusion of 246 $^1D_{NH}$ and 90 $^1D_{C\alpha H\alpha}$ residual dipolar coupling constraints (RDCs) (Fig. 1a). RDCs for residues with heteronuclear NOE values below 0.75 were not included in the structure calculations (i.e. for residues L3, E45, E46, E49, E62, H85, F87-E91). The addition of the RDC data into the structure calculations produced no NOE or dihedral angle violations and confirmed the accuracy of the original NOE-based structure (Drohat et al. 1998). As expected, the additional RDC constraints decreased the root mean squared difference (rmsd) for all ordered backbone atoms (1–88) from 1.2 to 0.8 Å in the 20 best structures, with Q-values lowering from 0.51 ± 0.05 in the original NOE-based structure to 0.19 ± 02 in the refined NMR structure (Table 1; Fig. 1b). The interhelical angles and distances were also unchanged within error upon addition of RDC data. While no differences in structure could be detected, the refined NMR structure reported here is better resolved and higher in quality than that originally published (Drohat et al. 1998).

^{15}N relaxation rate data for Ca^{2+}-S100B

It was observed that B-factor values in the X-ray crystal structure were elevated in several regions of Ca^{2+}-S100B (Matsumura et al. 1998), perhaps as a result of internal motion. Specifically, residues in helix 1 (K5, H15, Q16), the pseudo EF-hand (E21, K24, H25), loop 2 (i.e. the hinge region) (E45, E46, K48, and E49), the canonical EF-hand (S62, D63, G64), and in the C-terminus (E86, F87, F88) displayed B-factors that are more than 1.5 times higher than the standard deviation of the 10% trimmed mean (Fig. 3a). It was also observed that the largest differences observed between RDCs predicted by the X-ray structure and those measured by NMR occurred for most of these same residues. Furthermore, when these regions with elevated B-factors were not included in the Q-factor calculation, the quality factor for the X-ray structure improved from $Q = 0.45$ to $Q = 0.35$, providing additional evidence that these regions may exhibit internal dynamics. Therefore, NMR ^{15}N-relaxation data (R_1, R_2, and {^1H}-^{15}N NOE) were collected at 14.4 and 18.8 Tesla to more directly determine whether these and/or other regions of Ca^{2+}-S100B are mobile on one or more timescales.

Of the 91 backbone resonances in Ca^{2+}-S100B, ^{15}N-relaxation rate data were evaluated for 79 residues with the remaining 12 residues not analyzed either due to spectral overlap and/or because they were missing or very weak because of exchange broadening. The 10% trimmed mean values of the R_1 ($1/T_1$) values for the 79 observable correlations were 0.894 s^{-1} at 800 MHz and 1.275 s^{-1} at 600 MHz (Fig. 2a). For R_2, the trimmed means were 19.67 s^{-1} for 800 MHz and 15.32 s^{-1} for 600 MHz (Fig. 2b), and the NOE trimmed mean values were 0.835

Table 1 NMR-derived restraints and statistics of 20 NMR structures[a]

	<20>	Best
rmsd from distance constraints[b] (Å)		
Total (2,158)	0.015 ± 0.002	0.015
Intraresidue (372)	0.020 ± 0.005	0.021
Sequential ($\|i-j\|=1$) (556)	0.018 ± 0.003	0.018
Medium range ($1<\|i-j\|\leq 1$) (636)	0.006 ± 0.005	0.009
Long range ($\|i-j\|>5$) (258)	0.011 ± 0.003	0.012
Dimer interface (138)	0.014 ± 0.004	0.009
Intra-and/or intermolecular (26)	0.005 ± 0.007	0.000
Modeled calcium ligands (20)	0.010 ± 0.007	0.018
Hydrogen bonds (152)	0.007 ± 0.008	0.006
rmsd from exptl dihedral constraints (°)		
Φ,Ψ (122)	0.453 ± .155	0.248
rmsd from dipolar coupling restraints (Hz)		
D_{NH1} (118)	1.306 ± 0.017	1.180
D_{NH2} (128)	1.050 ± .004	1.040
D_{CH} (90)	3.060 ± 0.826	2.511
rmsd from exptl ^{13}C chemical shifts		
$^{13}C\alpha$ (ppm)	1.245 ± 0.041	1.231
$^{13}C\beta$ (ppm)	1.498 ± 0.042	1.560
rmsd from idealized geometry		
Bonds (Å)	0.002 ± 0.001	0.003
Angles (°)	0.388 ± 0.017	0.418
Impropers (°)	0.475 ± 0.032	0.519
Lennard-Jones potential energy (kcal/mol)[c]	−778 ± 38	−827
% of residues in the most favorable region of the Ramachandran plot[d]	89.7 ± 3.8	89.4
Bad contacts per 100 residues	7.4 ± 3.0	6
H-bond energy S.D.	0.93 ± 0.06	1.0
Overall dihedral *G* factor	0.35 ± 0.06	0.30
Q-factor[e]	0.19 ± 0.02	0.21
rmsd to the mean structure (Å)[f]		
All backbone atoms in S100B (1–88)	0.780 ± 0.056	0.666
All heavy atoms in S100B (1–88)	1.535 ± 0.081	1.475

[a] The 20 ensemble structures, <20>, are the results of simulated annealing calculations. The best structure is designated to be the structure that most closely resembles the average structure. The values shown for the <20> are the mean ± standard deviation

[b] None of the 20 structures has a distance violation >0.4 Å or a dihedral angle violation of >5°. The force constants used in the SA calculations are as follows: 1,000 kcal mol^{-1} $Å^2$ for bond length, 500 kcal mol^{-1} rad^{-2} for angles and improper torsions, 4 kcal mol^{-1} $Å^{-4}$ for the quartic van der Waals (vdw) repulsion term (hard-sphere effective vdw set to 0.8 times their values in CHARMm parameters), 50 kcal mol^{-1} $Å^{-2}$ for experimental distance constraints, 100 kcal mol^{-1} $Å^{-2}$ for non-crystallographic symmetry, 1.0 kcal mol^{-1} $Å^{-2}$ for distance symmetry constraints, 0.5 kcal mol^{-1} ppm^{-2} for the ^{13}C chemical shift constraints, and 1.0 for the conformational database potential. The force constants (in kcal Hz^{-2}) used for dipolar coupling restraints were as follows: 1.80 for ^{15}N-$^{1}H^{N}$ #1, 0.60 for ^{15}N-$^{1}H^{N}$ #2, and 0.15 for ^{13}C-$^{1}H^{\alpha}$

[c] Lennard-Jones van der Waals energies were calculated using CHARMm parameters and were not used in any stage of the structure determination

[d] PROCHECK was used to generate the Ramachandran plot

[e] The *Q*-factor was calculated twice and the average value is reported. In each calculation 10% of the C^{α}-H^{α} and N^{H}-H collected in the radially compressed gel were removed and used to determine the *Q*-factor (see text)

[f] Backbone calculations include C^{α}, N, and C′ atoms. Only residues 1–88 are included since no long-range NOE correlations were observed for residues 88–91

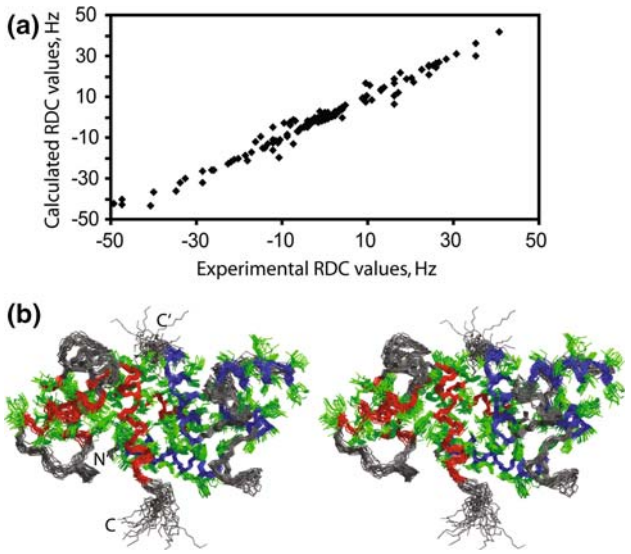

Fig. 1 Refined structure of rat Ca^{2+}-S100B using residual dipolar couplings. **a** Plot of calculated vs. experimental RDC for D_{NH} and $D_{C\alpha H\alpha}$, showing that the data fit the structure well. **b** Overlay of the 20 best Ca^{2+}-S100B structures in stereo view. Residues in helices are colored red in subunit 1 and blue in subunit 2. Side chains of ordered secondary structure are colored in green. All other residues in both subunits are colored in gray

for 800 MHz and 0.796 for 600 MHz (Fig. 2c). In addition to residues that were missing or visibly exchange broadened (residues S1, K5, G22, D23, K24, H42, F43, I47, K48, Q50, V80, T81, T82, H85, E86, and F87), several other residues (D12, H15, L44, A83, and C84) were also identified as having R_{ex} from a plot of residual dipolar couplings $^1D_{NH}$ versus T_1/T_2 ratio (Fig. 2d) (de Alba et al. 1999). Thus, residues located in helix 1 (K5, D12, H15), the pseudo EF-hand (G22, D23, K24), the hinge region (H42, F43, L44, I47, K48, Q50) and the C-terminal tail of S100B (V80, T81, T82, A83, C84, H85, E86, and F87) may be mobile on the chemical shift timescale, perhaps due to motion in the C-terminal loop (residues 84–91) as observed previously in apo-S100B (Inman et al. 2001) (Fig. 3b). In addition, several residues in the hinge region (E45, E46, E49) and the C-terminal loop (loop 4) of Ca^{2+}-bound S100B (H85, F87-E91) exhibited $\{^1H\}$-^{15}N NOE values that were below 0.75 at two field strengths indicating that these regions of the protein are also mobile on fast timescales (ns-ps; Fig. 3c).

In summary, helix 1 and all four loops in S100B likely have motion on fast and/or slow timescales as judged by NMR and supported by B-factors from X-ray crystallography. As was observed previously for apo-S100B (Inman et al. 2001), residues in C-terminal loop of Ca^{2+}-bound S100B are mobile on fast and perhaps slow timescales as judged by low heteronuclear NOE values (H85, F87-E91), exchange broadening effects (A83-F87), and elevated B-factors or no density in the X-ray crystal structure

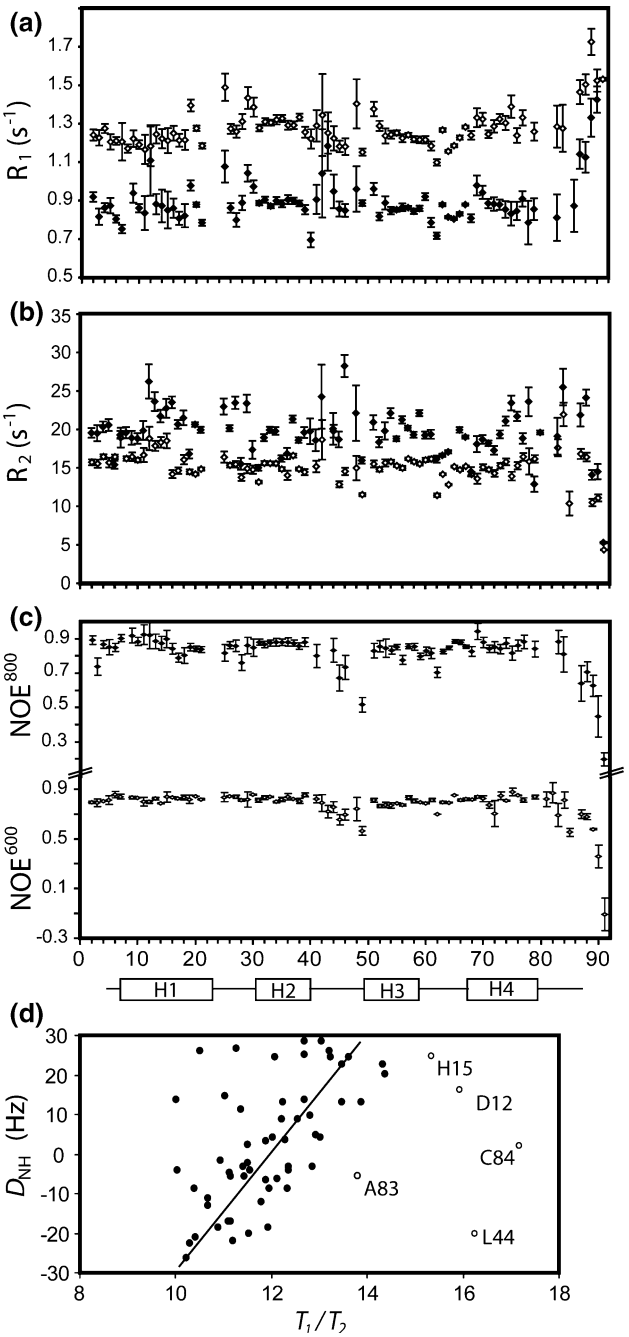

Fig. 2 ^{15}N-relaxation rate data for Ca^{2+}-S100B. **a** Longitudinal relaxation rate R_1, **b** transverse relaxation rate R_2, and **c** $\{^1H\}$-^{15}N heteronuclear NOE ($\eta + 1$) data are given for nitrogen Larmor frequencies of 81 MHz (solid diamonds) and 61 MHz (open diamonds). **d** Residual dipolar couplings, D_{NH}, plotted against ^{15}N T_1/T_2 ratios collected at 61 MHz; data included in the linear correlation are displayed as filled circles (●), and those considered outliers (>2× the standard deviation to the right of the best-fit line) as open circles (○)

(E86-E91). Similarly loop 2, termed the 'hinge region,' experiences fast-timescale dynamics for several residues (E45, E46, E49) in addition to having exchange broadening (E45, E46, K48, E49) and elevated B-factors (E45, E46,

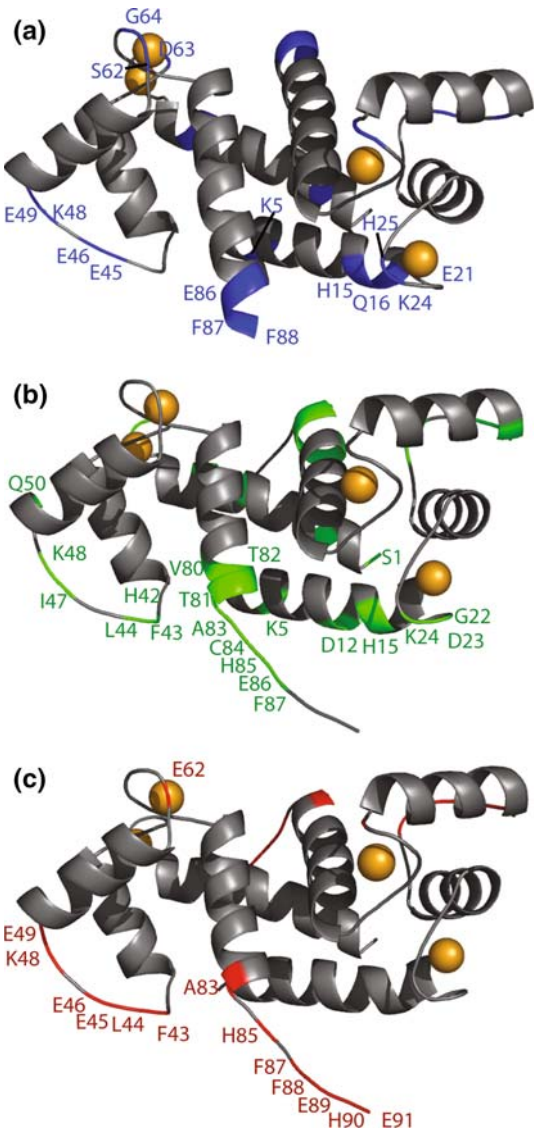

Fig. 3 Ribbon diagrams of Ca^{2+}-S100B illustrating elevated B-factors from the X-ray crystal structure and ^{15}N-relaxation rate data relevant to its dynamic properties on slow and fast timescales. **a** Residues with B-factors significantly larger than the average B-factor are mapped (in blue) onto the ribbon diagram for the X-ray structure of Ca^{2+}-S100B (PDB accession number 1MHO). **b** Residues for which chemical exchange is detected are mapped (in green) onto the refined solution NMR structure of Ca^{2+}-S100B. **c** Residues that have low $\{^1H\}$-^{15}N NOE values at 600 MHz, indicative of fast timescale motions, are mapped (in red) onto the refined solution NMR structure

K48, E49). It is noteworthy to point out that these same two regions of S100B (the hinge and the C-terminal loop) make up a large portion of the target protein binding site on S100B, so it is possible that the dynamic properties in these regions are functionally important since they may provide a means for S100B to interact with its diverse set of targets.

In addition to loops 2 and 4, three NH correlations for residues in helix 1 are exchange broadened (K5, D12, and H15) with L3 exhibiting a low heteronuclear NOE value (<0.75) and K5 having an elevated B-factor in the X-ray crystal structure; however, no other helix in S100B shows such features. While it is possible that these exchange broadening effects could result from movements of helix 1 on the chemical shift timescale, the extremely low S100B dimer dissociation constant suggests that this helix is quite stable; it is more likely that such exchange broadening results from the C-terminal loop approaching helix 1 as was observed in apo-S100B (Inman et al. 2001). Similarly, three residues in the loop of the pseudo-EF-hand have elevated B-factors (G22-K24) and/or exhibit exchange broadening effects by NMR (E21, K24, H25), which may also be the result of its proximity to the C-terminal loop. Lastly, several residues in the typical EF-hand (S62-G64) have elevated B-factors in the X-ray structure, and one residue (N62) exhibits a low heteronuclear NOE value. This result was somewhat surprising since N62 is in between two Ca^{2+}-liganding residues (D61 and D63). However, previous studies have shown that the Ca^{2+}-binding affinity of S100B is rather weak in comparison to other EF-hand proteins, but increases upon binding protein targets (Markowitz et al. 2005). These issues will make it interesting to determine whether the dynamic properties observed here for Ca^{2+}-S100B are eliminated upon binding a protein target since such an effect could provide a mechanistic explanation for how protein target binding can increase the affinity that S100B has for calcium.

Discussion and conclusions

The solution NMR structure of Ca^{2+}-S100B was refined by the inclusion of residual dipolar coupling data, which resulted in a higher quality ensemble of structures with lower backbone rmsd values (Table 1; Fig. 1). The comparison of this structure to that of S100B in the apo-state is important for fully understanding the Ca^{2+}-dependent conformational change in S100B that is necessary for it to bind its protein targets. As discovered for several S100 proteins so far, the rotation and conformational change of helix 3, brought about by calcium binding, is accompanied by breaking and forming numerous hydrophobic contacts in S100B (Wilder et al. 2006; Drohat et al. 1998; Smith and Shaw 1998). In the apo-form (Drohat et al. 1999), helix 3 and helix 4 are held together by a large hydrophobic strip of residues, consisting primarily of V53, V56, and L60 in helix 3, and F76, M79, V80, and A84 in helix 4. In contrast to the well-packed helix 3–4 interface, helices 2 and 3 do not pack together well in apo-S100B, primarily because of the position of the bulky M57, along with the presence of a charged residue (K33) in the middle of an otherwise hydrophobic area. Upon the addition of calcium, the large conformational change of helix 3 allows for

several residues in helix 3 (V56 and L60) to pack against helix 4 (F76 and M79), forming a smaller hydrophobic region. However, other residues, including V52, V80, and A83, no longer contribute to the helix 3–4 helix packing. On the opposite face of helix 3, the conformational change alters the residues of helix 3 that are located at the helix 2–3 interface; M57 is rotated to the periphery of this interface, and V57 and V53 exhibit much more contact with helix 2. Complementing this movement, the slight reorientation of helix 2, brought about by Glu-31 coordinating with calcium, presents a more hydrophobic side of helix 2 to helix 3; L32 and I36 are rotated into the helix interface, and importantly K33 is moved slightly out of this region. This allows for more substantial hydrophobic contact between the helices 2 and 3, without the destabilizing effect of a charged residue in this region. The presence of these hydrophobic interactions between helices 2 and 3 in the Ca^{2+}-bound state, most notably those between V53 and L32, is probably necessary to stabilize the open conformation of Ca^{2+}-S100B.

S100A1 and S100A6, two other S100 proteins for which both Ca^{2+}-loaded and apo structures are available, also exhibit poor helix packing between helices 2 and 3 in the apo form of the molecule. As is the case in S100B, this unfavorable packing is brought about by interactions between the bulky methionine at residue 57 and the charged lysine at position 33 (S100B numbering). Interestingly, the rotation of Lys-33 out of the helix 2–3 interface upon the addition of calcium is conserved among S100A1, S100A6, and S100B. Additionally, all three proteins retain a conserved leucine at residue 33 and a conserved valine at residue 53, and demonstrate similar sidechain orientations in the presence of calcium. Such helix packing in both the apo and the Ca^{2+}-bound form of S100 proteins is thus probably a common feature within this family of Ca^{2+}-binding proteins and could explain why little if any internal dynamics are observed for helical residues of Ca^{2+}-S100B.

The X-ray and the newly refined NMR structures of Ca^{2+}-S100B are nearly indistinguishable with the only difference being eight residues in the extreme C-terminus (residues C84-E91); the NMR shows this region to be largely unstructured while the X-ray structure shows this area to be helical. Examination of ^{15}N-relaxation rates resolved this discrepancy, since these data demonstrated that the C-terminus of Ca^{2+}-S100B (residues A83 to E91) is mobile on fast timescales (ps-ns) in solution and several residues in this region also exhibit exchange broadening effects consistent with motion on slow timescales (μs-ms). However, it is important to note that the presence of target peptide induces the same helix 4 extension in solution as was reported for crystallized Ca^{2+}-S100B (Inman et al. 2002; Matsumura et al. 1998; Rustandi et al. 2000); therefore, the extended helix 4 observed in the crystal structure may be an effect of crystal contacts that mimic target protein binding.

The refined NMR structure of Ca^{2+}-bound S100B and the accompanying ^{15}N-relaxation rate data provide the foundation for more complete analyses of the dynamic properties of the protein in this state as well as for making detailed comparisons of S100B in the apo-, Ca^{2+}-bound, and target-bound forms. In summary, the results presented here provide evidence that residues at the C-terminus of Ca^{2+}-S100B (A83-E91), as well as several residues in loop 2 (termed the hinge region), are dynamic in solution. The unstructured, flexible regions we have observed for the hinge (loop 2) and loop 4 are likely to be important for accommodating the binding of wide variety of proteins to Ca^{2+}-S100B. Because of the high degree of structural and sequence homology, similar dynamic regions may be present in other S100 proteins. In fact, the Ca^{2+}-bound form of both S100A1 and S100A6 demonstrate increased rmsd in the hinge region and the C-terminus, presumably due to fewer NOE correlations perhaps caused by a higher degree of residue mobility (Wright et al. 2005; Mäler et al. 2002). In order to assess the interplay between structure, dynamics and target binding, it is important to extend NMR studies of Ca^{2+}-S100B to also include target peptide(s) complexes as well as to other S100 proteins to determine whether the features observed here for Ca^{2+}-S100B are common throughout the S100 protein family.

Acknowledgements This work was supported by a grant from the National Institutes of Health (GM58888; CA107331 to DJW). The NMR spectrometers used in these studies were purchased, in part, with funds from shared instrumentation grants from the NIH (S10 RR10441; S10 RR15741; S10 RR16812; S10 RR23447 to DJW) and from the NSF (DBI 0115795 to DJW). NTW was partially supported by NIAMS training grant T32 AR007592 to the Interdisciplinary Program in Muscle Biology, University of Maryland School of Medicine, and by an American Heart Association training grant 0615343U.

References

Bax A, Kontaxis G, Tjandra N (2001) Dipolar Couplings in macromolecular structure determination. Methods Enzymol 339:127–174

Charpentier TH, Wilder PT, Liriano MA, Varney KM, Pozharski E, Mackerell AD Jr, Coop A, Toth EA, Weber DJ (2008) Divalent metal ion complexes of S100B in the absence and presence of pentamidine. J Mol Biol 382(1):56–73

de Alba E, Baber JL, Tjandra N (1999) The use of residual dipolar couplings in concert with backbone relaxation rates identify conformational exchange by NMR. JACS 121:4282–4283

Delaglio F, Grzesiek S, Vuister GW, Zhu G, Pfeifer J, Bax A (1995) NMRPipe: a multidimensional spectral processing system based on UNIX pipes. J Biomol NMR 6:277–293

Drohat AC, Baldisseri DM, Rustandi RR, Weber DJ (1998) Solution structure of calcium-bound rat S100B(betabeta) as determined by nuclear magnetic resonance spectroscopy. Biochemistry 37:2729–2740

Drohat AC, Tjandra N, Baldisseri DM, Weber DJ (1999) The use of dipolar couplings for determining the solution structure of rat apo-S100B(betabeta). Protein Sci 8:800–809

Heizmann CW, Ackermann GE, Galichet A (2007) Pathologies involving the S100 proteins and RAGE. Subcell Biochem 45:93–138

Inman KG, Baldisseri DM, Miller KE, Weber DJ (2001) Backbone dynamics of the calcium-signaling protein apo-S100B as determined by 15N NMR relaxation. Biochemistry 40:3439–3448

Inman KG, Yang R, Rustandi RR, Miller KE, Baldisseri DM, Weber DJ (2002) Solution NMR structure of S100B bound to the high-affinity target peptide TRTK-12. J Mol Biol 324:1003–1014

Lin J, Yang Q, Yan Z, Markowitz J, Wilder PT, Carrier F, Weber DJ (2004) Inhibiting S100B restores p53 levels in primary malignant melanoma cancer cells. J Biol Chem 279:34071–34079

Mäler L, Sastry M, Chazin WJ (2002) A structural basis for S100 protein specificity derived from comparative analysis of apo and Ca^{2+}-calcyclin. J Mol Bio 317:279–290

Markowitz J, Rustandi RR, Varney KM, Wilder PT, Udan R, Wu SL, Horrocks WD, Weber DJ (2005) Calcium-binding properties of wild-type and EF-hand mutants of S100B in the presence and absence of a peptide derived from the C-terminal negative regulatory domain of p53. Biochemistry 44:7305–7314

Matsumura H, Shiba T, Inoue T, Hurada S, Kai Y (1998) A novel mode of target recognition suggested by the 2.0 A structure of holo S100B from bovine brain. Structure 6:233–241

Rustandi RR, Baldisseri DM, Weber DJ (2000) Structure of the negative regulatory domain of p53 bound to S100B(betabeta). Nat Struct Biol 7:570–574

Salama I, Malone PS, Mihaimeed F, Jones JL (2008) A review of the S100 proteins in cancer. Eur J Surg Oncol 34:357–364

Smith SP, Shaw GS (1998) A novel calcium-sensitive switch released by the structure of human S100B in the calcium-bound form. Structure 6:211–222

Tjandra N, Omichinski JG, Gronenborn AM, Clore GM, Bax A (1997) Use of dipolar 1H–15N and 1H–13C couplings in the structure determination of magnetically oriented macromolecules in solution. Nat Struct Biol 4:732–738

Wilder PT, Lin J, Bair CL, Charpentier TH, Yang D, Liriano M, Varney KM, Lee A, Oppenheim AB, Adhya S, Carrier F, Weber DJ (2006) Recognition of the tumor suppressor protein p53 and other protein targets by the calcium-binding protein S100B. Biochim Biophys Acta 1763:1284–1297

Wright NT, Varney KM, Ellis KC, Markowitz J, Gitti RK, Zimmer DB, Weber DJ (2005) The three-dimensional solution structure of Ca(2+)-bound S100A1 as determined by NMR spectroscopy. J Mol Biol 353:410–426

Wright NT, Prosser BL, Varney KM, Zimmer DB, Schneider MF, Weber DJ (2008) S100A1 and calmodulin compete for the same binding site on ryanodine receptor. J Biol Chem 283(39):26676–26683